DRAFT VERSION

ELECTRONIC TEMPERATURE MEASUREMENT BY JOHNSON NOISE THERMOMETRY: DETERMINING BOLTZMANN'S CONSTANT

EDITION 2017

Samuel P Benz[2], Kevin Coakley[2], Nathan Flower-Jacobs[2], Jifeng Qu[1], Horst Rogalla[2,3], Weston L Tew[4], D Rod White[5], Kunli Zhou[1] and Zhenyu Zhou[1]

[1]*National Institute of Metrology (NIM), Beijing 100029, People's Republic of China*
[2]*National Institute of Standards and Technology (NIST), 325 Broadway, Boulder, CO 80305-3328, USA*[1]
[3] *ECEE Department, University of Colorado at Boulder, Boulder, CO 80303*
[4] *National Institute of Standards and Technology (NIST), 100 Bureau Drive, Gaithersburg, MD 20899, USA*
[5]*Measurement Standards Laboratory of New Zealand, Lower Hutt, New Zealand*

Introduction

In 2018, the unit of thermodynamic temperature, the kelvin, will be redefined with the introduction of the 'New SI' (New International System of units), by fixing the value of the Boltzmann constant, *k* [1]. To assure that there are no large unknown systematic effects in determining the value of *k* by any single technique, the Consultative Committee for Thermometry (CCT) of the International Committee for Weights and Measures (CIPM) requires that the kelvin redefinition should proceed when the next CODATA adjustment assigns a value of *k* with a relative uncertainty below $1{\cdot}10^{-6}$, supported by at least one determination from a second technique reporting a relative uncertainty below $3{\cdot}10^{-6}$ [2]. Two determinations by acoustic gas thermometry have already achieved relative uncertainties less than $1{\cdot}10^{-6}$ so the current CODATA recommended value of *k* has met the first requirement [3-5]. To meet the second requirement, at least three different research groups have been pursuing determinations of *k* with a relative uncertainty less than $3{\cdot}10^{-6}$ using dielectric-constant gas thermometry (DCGT) [6-7], Doppler broadening thermometry (DBT) [8-9], and Johnson noise thermometry (JNT) [10-12]. The second target has been met by PTB who recently reported a determination by DCGT with a relative uncertainty of $1.9{\cdot}10^{-6}$ [13]. Here we report on Johnson noise thermometry to determine the Boltzmann constant, which recently met the 3 ppm-target in measurements carried out at NIM within the joint NIST/NIM/MSL collaboration [14]. This result, which is purely electronic and distinctly different from the gas thermometry determinations, provides additional assurance that any unknown systematic errors in any of the determinations must be small.

Johnson noise thermometry infers the thermodynamic temperature from measurements of the voltage or current noise caused by the thermal motion of electrons in conductors [15-17]. Similar to gas thermometry, the Johnson noise fundamental relation follows from the fluctuation-dissipation theorem relating the electron gas temperature directly to voltage noise. As a purely electronic approach, JNT has attracted the attention of physicists and metrologists over many years. Still, even

with modern electronic measurement systems, the amplification of small and wideband noise-voltages for the determination of k is not trivial and requires correlation techniques and nearly perfect shielding since EMI in cross-correlation channels can influence the measurement. Over the years, an elaborate analysis technique has been developed, which recently was further improved by the cross-validation method developed at NIST [18].

In the following 6 sections, we will introduce the principles of the Johnson noise thermometry, the experimental and analysis techniques, and finally results of the measurement and their uncertainty.

Johnson noise temperature measurement system

Johnson noise is usually characterized by its mean square voltage, conventionally called the noise power. For frequencies below 1 MHz and temperatures above 25 K, it is approximated to better than 1 part in 10^6 by Nyquist's equation,

$$\langle V^2 \rangle = 4kTR\Delta f, \tag{1}$$

where k is Boltzmann's constant, T is the temperature of the resistance R, and Δf is the measurement bandwidth. Johnson-Nyquist noise is often described as a "white noise", since the power spectral density (PSD) $S_R = 4kTR$ is independent of frequency. Because the fluctuation-dissipation theorem is fundamental, Johnson noise thermometers (JNT) are primary thermometers measuring "absolute" thermodynamic temperatures. The most significant measurement challenge of JNT is apparent from (1), namely that the noise voltages are extremely small, ~1.2 nV/Hz$^{1/2}$, for a 100 Ω resistor at the triple point of water. Very-high-performance electronics, cross-correlation measurement techniques, and long averaging times are required to make metrologically useful JNT measurements [19] (for an extensive JNT review see [20]).

In conventional JNT systems, one measures the noise power from a sensor at a known temperature (often the triple point of water, which conveniently has a defined temperature in the International System of Units: $T_w \equiv 273.16$ K) and the noise power of a second sensor at the unknown temperature. The temperature is inferred using (1) from the ratio of the measured noise powers and the ratio of the sensing resistances. The most successful JNT technique for the medium- and high-temperature ranges is the switched-input correlator pioneered by Brixy for application in nuclear reactors [21] and is now used routinely for most metrological noise thermometry. It combines the amplifier-noise immunity of cross-correlators, first used by Fink [22], and the gain-instability immunity of the Dicke radiometer [23].

The most accurate noise thermometers are based on a switching-correlator design first proposed by Brixy [19, 20]. A correlator is used to ensure that the measurement of the noise power is independent of the input noise voltage of the preamplifiers. Frequent switching between two noise sources, eliminates the effects of drifts in the gain and frequency response of the two channels. The correlator is implemented by digitizing the amplified signals from two correlator channels and followed by multiplication and averaging operations via software.

Modern JNT systems use a switched digital cross-correlator and a programmable quantized-voltage noise source (QVNS) based on ac-Josephson voltage standards as a calculable noise reference [24-28]. This enables the correlator to compare the power spectral density of the thermal noise of the resistor at the triple point of water with the quantum-mechanically stable synthetic noise generated

by the QVNS, and infer a value of k/h [29,12].

Quantum voltage noise source

The Quantum Voltage Noise Source (QVNS) is a Josephson-junction-based delta-sigma digital-to-analog converter that uses oversampling techniques to produce a programmed sequence of pulses clocked at >= 5 GHz [27,30]. With appropriate algorithms and biasing, it produces a pseudo-noise waveform with the desired harmonic content over a baseband well beyond the <10 MHz bandwidth of the JNT. The primary advantage of the QVNS is that the voltage pulse from each Josephson junction has a quantized area $nh/2e=nK_J$, where n is an integer (normally n = 1 in the NIST QVNS) and K_J is the Josephson constant. This enables the synthesized baseband voltage to be calculated exactly from the known sequence of pulses, the clock frequency of the pulse generator, and fundamental physical constant.

The synthesis technique underlying the QVNS was originally developed for ac-Josephson voltage standards [31]. However, the low voltages and long integration times of noise thermometry necessitate a specialized QVNS circuit consisting of a pair of symmetric, grounded, lumped arrays, having only a small number of junctions (typically N_J = 8 to 256). The quantum-accurate pseudo-noise output voltage from the series-connected arrays is provided to the two channels of the cross-correlation electronics through a pair of three-wire grounded differential output voltage leads. The four impedance-matching resistors terminating the QVNS transmission line are placed in each lead of the transmission line so that they produce only uncorrelated noise, and are maintained at 4 K so that they do not unduly increase the uncorrelated noise in each channel of the correlator.

Each array is separately biased with a continuously recycled pulse drive sequence that is clocked at half the 10 GHz sampling frequency, f_s. To reduce inductive voltage errors caused by low-frequency drive currents passing through the inductive JJ arrays, a zero-compensation technique is used where each drive pulse is composed of a negative half-pulse followed by a full positive pulse followed by another negative half-pulse. This composite drive pulse can still force each JJ to create a single positive output pulse, but does not have any low-frequency components [32,33]. The drive sequence, M composite pulses long, is generated with a delta-sigma analog-to-digital conversion algorithm that is programmed to produce a synthesized waveform with the desired and precisely calculable power spectrum. The spectrum is composed of a series of tones at multiples of the pattern repetition frequency, $f_1 = f_s/M \approx 100$ Hz. The usual JNT waveform is a series of tones at the odd harmonics f_1, $3f_1$, $5f_1$,…, all of the same amplitude but random phase. When used to measure k, the voltage amplitude of the tones is adjusted by changing the pulse sequence so that the synthesized waveform's average power spectral density $S_Q = D^2N_J^2f_sM/K_J^2$ matches the thermal noise power spectral density, $S_R=4kTR$, where D is a precisely known parameter that is chosen to closely match the QVNS power spectral density to that of the resistor $S_Q \approx S_R$,

In addition to providing the link to Planck's constant, the QVNS has important advantages over resistor noise sources [20]. Unlike a resistor noise source, the QVNS output voltage is inherently independent of its output impedance. This overcomes the matching conflict inherent in conventional Johnson noise thermometers. Now, the thermal and QVNS sources have the same noise power, in order to minimize effects of any amplifier or ADC nonlinearity. An output resistance is chosen to ensure the same frequency responses of the transmission lines between the resistor and QVNS sources and the preamplifiers. This reduces the 'spectral match' error and allows a reduced

measurement period due to a greater operating bandwidth. The QVNS can also be programmed to produce a variety of different waveforms for diagnostic purposes. In contrast, the noise power and impedance cannot be independently varied in a conventional Johnson noise thermometer, resulting in some degree of mismatch of frequency response and noise power between measurement and reference sensors.

Measurement of Boltzmann's constant – Experiment

To measure the Boltzmann constant, the JNT runs as a comparator to compare the power of thermal noise across a sense resister immersed in a triple point of water cell to that of a synthesized comb-like quantum pseudo noise waveform. The power spectral density of the quantum pseudo noise waveform, $S_{\text{Q-calc}}$, was set to closely match that of the thermal noise S_{R}, so that problems with linearity and accuracy of the electronics can be greatly reduced.

The two correlator channels alternately amplify, filter, and sample the respective noise signals from the thermal and QVNS sources, which are then digitized by the ADCs, Fourier transformed, and cross-correlated in software. The output of the correlator is proportional to the noise powers of the respective thermal and QVNS signals. Since the bandwidth of the system is defined digitally and is the same in the two configurations, the ratio of the cross-correlated discrete-Fourier transforms for each source yields the measured ratio of the power spectral densities S_R/S_{Q}. The Boltzmann constant is then determined by

$$k = \frac{S_R}{S_{\text{Q}}} \times \frac{S_{\text{Q-calc}}}{4T_{\text{TPW}}R} \times \frac{h}{h_{90}}, \qquad (2)$$

where $S_{\text{Q-calc}}$ is the calculated power spectral density of the quantum noise waveform, T_{TPW} is the temperature of triple point of water, R is the resistance of the thermal sensor, h and h_{90} are the Planck's constant in the SI and the 1990 conventional electrical units, respectively.

For the recent measurement at NIM, a 100 Ω metal foil resistor was used as thermal noise sensor. The QVNS waveform comprises a series of odd harmonic tones with the same amplitude but random phase at multiples of the 90 Hz pattern repetition frequency up to 9 MHz with $S_{\text{Q-calc}}$ = 1.2282 nV/Hz$^{1/2}$. The ADCs digitize the amplified noise signal with a sampling frequency of 4 MHz. For every 1 s, FFT of the signals are computed yielding complex spectra with 1 Hz frequency-resolved FFT bins and a 2 MHz Nyquist frequency. To ensure that the QVNS tones are located in a single FFT bin, the ADC clocks are locked to the same frequency reference as the QVNS clock. In addition to the FFTs, the computer carries out a complex frequency-domain cross correlation of the FFT spectra for the two channels, which reduces the uncorrelated amplifier noise voltages. All of these spectra are then accumulated for 100 s into averaged spectra to provide a compact form of data storage for post processing and for final computation. These computations are carried out in real time, and every 100 s, the correlator is switched between the resistor and the QVNS. The combination of 100 s of resistor data and 100 s of QVNS data is defined as one 'chop'.

Individual measurements were performed, each having an integration period of about 20 hours, which is determined by the capacity of the batteries for the digitizers and the maintenance period of the triple point of water cell in the ice bath. In total 120 such measurements were completed to reduce the statistical uncertainty, such that the combined total integration period of about 100 days were accumulated with 43752 chops of data. The resistance value of the sense resistor was checked before and after every measurement with a dc resistance bridge.

Once the measurements are complete, all of the cross-correlation spectra, 43752 chops of data for both of the thermal and QVNS sources, are averaged respectively. The real part of each of the thermal and QVNS cross-spectra are reduced in resolution by summing the 180 FFT bins, to form a spectral 'block'. This rebinning is necessary because most of the bins in the QVNS spectrum are largely empty due to the absence of the tones, and a direct ratio of the QVNS and thermal spectra would not have similar ratios in each bin. The ratio of the rebinned thermal and QVNS spectra is then computed.

Measurement of Boltzmann's constant – Analysis

For temperatures near 300 K and frequencies below 1 GHz, the mean-square voltage of Johnson noise is described by Nyquist's law, Equation (1), with a relative error of less than $1{\cdot}10^{-9}$. In the electronic measurement, the ratio of the power spectral densities of thermal noise across a resistor at the triple point of water and pseudo-random noise synthetically generated by a quantum-accurate voltage-noise source (QVNS) is determined. Given knowledge of this ratio, and the values of other parameters that are known or measured, one can determine Boltzmann's constant. Due, in part, to mismatch between transmission lines, the experimental ratio spectrum varies with frequency. We model the ratio of the power spectral densities of resistor noise and QVNS noise, $r_{model}(f)$, as a *d*th order even polynomial function of frequency as follows $r_{model}(f) = \sum_{i=0}^{i_{max}} \alpha_{2i} \left(\frac{f}{f_0}\right)^{2i}$ where $d = 2i_{max}$ and f_0 is a reference frequency. From the constant term in the polynomial model a_0 we determine Boltzmann's constant and compare it with a reference value $a_{0,calc}$. When determining a_0 from experimental data, the assumed order *d* (complexity) of the polynomial model and the maximum frequency analyzed (fitting bandwidth or f_{max} for short) dramatically affects results. For any particular fitting bandwidth, we select the complexity of the model by cross-validation - a data-driven machine learning method.

In our cross-validation approach, we randomly split observed spectra data from multiple runs of the experiment into 5 equally sized subsets. Data from each run appears in just one of the 5 subsets. From these subsets, we form training and validation data sets, and select the order of the model determined from training data which is most consistent with validation data according to mean-square deviation criterion. Based on 20 000 splits, we determine model selection fractions for all the candidate models. The orders of candidate models are 2, 4, 6, 8, 10, 12 and 14. We select the model that yields the largest model selection fraction.

Given that a *d*th order model is valid and *d* is known, asymptotic theory predicts a sampling distribution for the estimate of a_0. The standard deviation of this sampling distribution is the random uncertainty of the estimate predicted by asymptotic theory. To account for the effect of imperfect knowledge of the model on results, we form a mixture of the sampling distributions from the candidate models weighted by their associated model selection fractions determined by cross-validation. We estimate the uncertainty of estimated a_0 as the standard deviation of the mixture model distribution $\hat{\sigma}_{tot}$ where

$$\hat{\sigma}_{tot}^2 = \sum_d \hat{p}(d)\hat{\sigma}_{\hat{a}_0(d),ran}^2 + \sum_d \hat{p}(d)(\hat{a}_0(d) - \hat{\bar{a}}_0)^2 \,. \quad (3)$$

Above, $\hat{a}_0(d)$ is the estimate of a_0 associate with a *d*th order model, $\hat{\sigma}_{\hat{a}_0(d),ran}^2$ is the predicted variance of the estimate according to asymptotic theory, $\hat{p}(d)$ is the estimated model selection fraction for the *d*th order model, and $\hat{\bar{a}}_0 = \sum_d \hat{a}_0(d)\hat{p}(d)$.

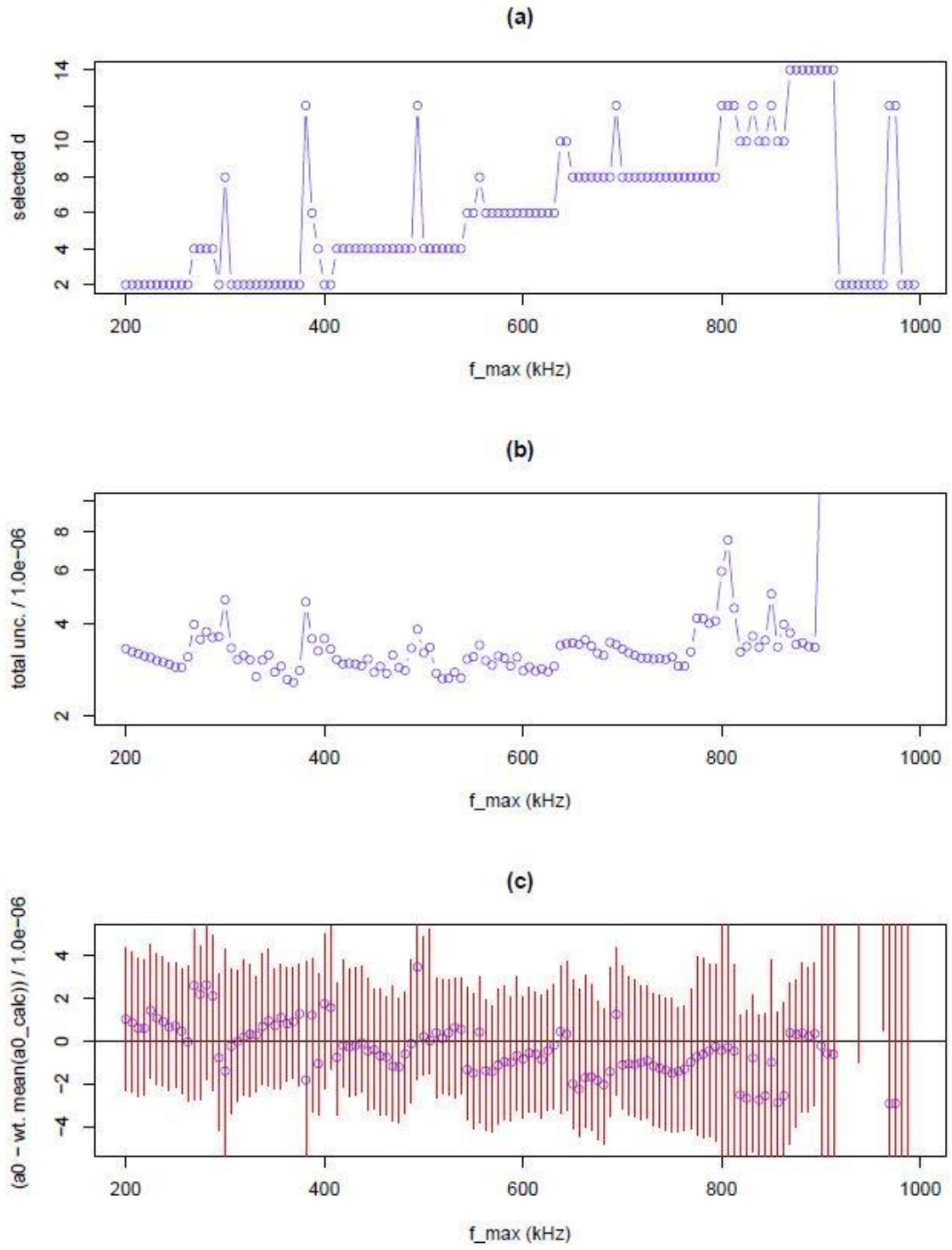

Fig. 1: Model selection results for experimental data from Qu et al. [14]. (a) Estimated polynomial complexity parameter *d*. (b) Estimated uncertainty $\hat{\sigma}_{tot}$. (c) Estimated $a_0 - a_{0,calc}$ and approximate 68 % coverage interval as a function of fitting bandwidth. At f_{max} = 368.75 kHz for a *d*=2 (quadratic) model, $\hat{\sigma}_{tot}$ takes its minimum value (on a frequency grid with a 6.25 kHz resolution) of $2.58 \cdot 10^{-6}$. For this selected fitting bandwidth, the estimated value of $a_0 - a_{0,calc}$ is $0.89 \cdot 10^{-6}$. Based on the estimated standard deviation of estimated a_0 values determined at f_{max} values that yield the thirteen (approximately 10 percent of all fitting bandwidths) lowest value of $\hat{\sigma}_{tot}$, we estimate an additional component of uncertainty due to fitting bandwidth ambiguity to be $0.57 \cdot 10^{-6}$.

We then select f_{max} by minimizing $\hat{\sigma}_{tot}$ on a uniformly spaced grid in frequency space. We also estimate an additional component of uncertainty that accounts for uncertainty associated with imperfect performance of our fitting bandwidth selection method. The sources of this imperfection include both random effects as well as systematic effects including possible frequency-dependent physical effects. We equate this additional component of uncertainty to the estimated standard deviation of estimated a_0 values determined at the f_{max} values that yield the *M* lowest values of $\hat{\sigma}_{tot}$. Typically, we set *M* so that it is approximately 0.1 N_f where N_f is number of discrete f_{max} values in our frequency grid. For more details about our model selection and uncertainty quantification methods, see [18].

Uncertainty Budget

Table 1: Uncertainty budget. All uncertainties are expressed as relative uncertainties in parts per million. The uncertainty budget for the 2015 determination is given for comparison.

Component	Term	Relative uncertainty		Correlation
		2015	2017	
Ratio of the power spectral densities, S_R/S_Q	Statistical	3.2	2.37	0
	Model Ambiguity	1.8	1.02	0
	Bandwidth Ambiguity	NA	0.57	0
	Dielectric losses	1.0	0.2	0
	EMI	0.4	0.4	0
	Non-linearity	0.1	0.1	1
	Total $u_r(S_R/S_Q)$	3.8	2.68	
QVNS waveform S_Q	Frequency reference	< 0.001	< 0.001	1
	Quantization effects	0.1	0.1	1
	Total(S_Q)	0.11	0.11	
TPW temperature *T*	Reference standard TPW cell	0.29	0.29	1
	Temperature measurement	0.04	0.04	1
	Hydrostatic pressure correction	0.08	0.08	1
	Immersion effects	0.18	0.18	1
	Total $u_r(T_W)$	0.35	0.35	
Resistance *R*	Ratio measurement	0.05	0.05	0
	Transfer Standard	0.1	0.1	1
	Ac-dc difference	0.1	0.1	1
	Relaxation effect	0.5	0.1	1
	Thermoelectric effect	0.1	0.1	1
	Total $u_r(R)$	0.53	0.21	
	TOTAL (k_B)	3.9	2.7	

All the factors that contribute to the total uncertainty were analysed in detail in the 2015 determination [12]. In the new measurement [14], for the terms such as the power spectral density S_Q of the synthesized quantum voltage waveform, the temperature of triple point of water, and some of the contributions to the uncertainty in the ratio of the power spectral densities S_R/S_Q and the resistance of thermal sensor are unchanged.

Discussion of Systematic Errors

The measurement of the mean ratio of spectral power spectral densities S_R/S_Q can be shifted under the influence of electromagnetic interference (EMI), preamplifier imperfections, or by various sources of spectral aberrations.

In the case of EMI, it is mainly necessary to access the presence of interference that is coupled to the resistor input and superimposed onto the white noise of the resistor. EMI with enough amplitude to contribute to errors greater than about 1 ppm may be present but would be too small to be spectrally resolvable in the normal measurement scheme. Fortunately, techniques are established [34] which involve a separate series of null measurements that allow quantitative evaluation of the EMI contributions in the resistor by rewiring the resistor into a four-wire short. EMI that may be coupled into the QVNS is more readily subject to direct inspection due to the nature of the QVNS source and the discrete spectra. EMI may be evaluated by comparison of that spectra with and without the 4 K background noise present between the tones.

Various preamplifier imperfections may lead to subtle errors in the measured spectral ratio. These have been treated by White and Zimmermann [35], and by White [36]. When the preamplifier is properly designed, all these sources of error should be manageable or negligible. Amplifier distortion is also a possibility which, if present, will eventually cause the statistical uncertainty to saturate to a fixed limit with accumulated integration time.

Spectral aberrations are a category which includes all potential sources of frequency dependence which cannot be modelled by the even-order filter-response functions that are normally used to fit the ratio spectra and are not caused by EMI or by amplifier distortion. This would include: sources of quasi-linear frequency dependence due to dielectric loss in shunt capacitance and unintentional local resonances in the input circuits. These errors would normally be captured in the statistical analysis and estimated by the model ambiguity uncertainty or bandwidth ambiguity uncertainty. In the case of a lossy dielectrics, auxiliary measurements may be necessary to set bounds on the magnitude of the losses and run statistical simulations to evaluate the errors via equivalent circuit models [26].

Other types of systematic errors may occur in either temperature or resistance. Resistance measurement errors may occur in either DC or AC measurements and have been discussed in [29]. Temperature errors associated with the direct use of triple-point-of-water (TPW) cells are generally known and can be empirically evaluated to auxiliary measurements using standard platinum resistance thermometers and other TPW cells.

References

[1] Mills I M, Mohr P J, Quinn T J, Taylor B N, and Williams E R 2006 Redefinition of the kilogram, ampere, kelvin and mole: a proposed approach to implementing CIPM recommendation 1 (CI-2005), *Metrologia*, vol. 43, pp. 227-46.

[2] Fischer J, *et al.*, the CCT report to the CIPM in 2014, BIPM, Sevres, France, 2014.

[3] de Podesta M, Underwood R, Sutton G, Morantz P, Harris P, Mark D F, Stuart F M, Vargha G, Machin G 2013 *Metrologia* vol. 50, pp. 354-76

[4] Michael de Podesta, Inseok Yang, Darren F Mark, Robin Underwood, Gavin Sutton and Graham Machin 2015, Correction of NPL-2013 estimate of the Boltzmann constant for argon isotopic composition and thermal conductivity, *Metrologia*, vol. 52, pp. S353-63.

[5] Pitre L, Sparasci F, Truong D, Guillou A, Risegari L, and Himbert M E 2011 Determination of the Boltzmann constant using a quasi-spherical acoustic resonator, *Int. J. Thermophys.,* vol. 32, pp. 1825-86.

[6] Gaiser C, Zandt T, Fellmuth B, Fischer J, Jusko O, and Sabuga W 2013 Improved determination of the Boltzmann constant by dielectric-constant gas thermometry, *Metrologia*, vol. 50, pp. L7-L11.

[7] Zandt T, Sabuga W, Gaiser C, and Fellmuth B, 2015 Measurement of pressures up to 7 Mpa applying pressure balances for dielectric-constant gas thermometry, Metrologia, vol. 52, pp. S305-13.

[8] Fasci E, Domenica De Vizia M, Merlone A, Moretti L, Castrillo A and Gianfrani L, 2015 The Boltzmann constant from the $H_2{}^{18}O$ vibration-rotation spectrum: complementary tests and revised uncertainty budget, Metrologia, vol. 52, pp. S233-41.

[9] S Mejri, P L T Sow, O Kozlova, C Ayari, S K Tokunaga, C Chardonnet, S Briaudeau, B Darquié, F Rohart and C Daussy, 2015 Measureing the Boltzmann constant by mid-infrared laser spectroscopy of ammonia, Metrologia, vol. 52, pp. S314-23.

[10] Benz S P, Pollarolo A, Qu J F, H Rogalla, Urano C, Tew W L, Dresselhaus P D, and White D R 2011 An electronic measurement of the Boltzmann constant, *Metrologia*, vol. 48, pp. 142-153.

[11] Qu J F, Fu Y F, Zhang J Q, Rogalla H, Pollarolo A, and Benz S P 2013 Flat frequency response in the electronic measurement of the Boltzmann constant measurement, *IEEE Trans. Instrum. Meas.*, 62 (6), 1518-1523.

[12] Qu J F, Benz S P, Pollarolo A, Rogalla H, Tew W L, White R D, and Zhou K L, 2015, Improved electronic measurement of the Boltzmann constant by Johnson noise Thermometry, Metrologia v. 52, pp. S242–S256, Aug. 2015

[13] Gaiser C, Fellmuth B, Haft N, Kuhn A, Thiele Krivoi, B, Zandt T, Fischer J, Jusko O, and Sabuga W, 2017, Final determination of the Boltzmann constant by dielectric constant gas thermometry, *Metrologia,* vol. 54, 280-289

[14] Qu J, Benz S P, Coakley K, Rogalla H, Tew W L, White D R, Zhou K and Zhou Z, An improved electronic determination of the Boltzmann constant by Johnson noise thermometry, to be published

[15] Johnson J B 1927 Thermal Agitation of Electricity in Conductors, *Nature* 119 50-51.

[16] Johnson J B 1928 Thermal Agitation of Electricity in Conductors, *Phys. Rev.* 32 97-109.

[17] Nyquist H 1928 Thermal Agitation of Electric Charge in Conductors, *Phys. Rev.* 32 110-113.

[18] Coakley K J and Qu J, Spectral model selection in the electronic measurement of the Boltzmann constant by Johnson noise thermometry, *Metrologia* vol. 54, p.204.

[19] Webb R A, Giffard R P, Wheatley J C, Noise thermometry at ultralow temperatures, J. Low Temp. Phys. 13 (1973) 383–429.

[20] White D R, Galleano R, Actis A, Brixy H, De Groot M, Dubbeldam J, Reesink A L, Edler F, Sakurai H, Shepard R L and Gallop J C, The status of Johnson noise thermometry, Metrologia 33 (1996) 325-335.

[21] Brixy H, Hecker R, Oehmen J, Rittinghaus K F, Setiawan W, Zimmermann E, Noise thermometry for industrial and metrological applications at KFA Jülich, in: J. F. Schooley (Ed.), Temperature, Its Measurement and Control in Science and Industry 6, Am. Inst. Phys., New York, 1992, pp. 993-996.

[22] Fink H J, A new absolute noise thermometer at low temperatures, Can. J. of Phy. 37 (1959) 1397-1406.

[23] Dicke R H, "The measurement of thermal radiation at microwave frequencies", Rev. Sci. Inst. vol. 17, pp. 268-275 (July 1946).

[24] Benz S P, Martinis J M, Nam S W, Tew W L, and White D R, A new approach to Johnson noise thermometry using a Josephson quantized voltage source for calibration, *Proceedings of TEMPMEKO 2001*, (Edited by B. Fellmuth, J. Seidel, and G. Scholz) VDE Verlag, Berlin, 2002, 37-44.

[25] Benz S P, Dresselhaus P D, and Martinis J, An ac Josephson source for Johnson noise thermometry, *IEEE Trans. Inst. Meas.*, 2003, **IM-52**, 545-549.

[26] Tew W L, Benz S P, Dresselhaus P D, Rogalla H, White D R, and Labenski J R, “Recent Progress in noise thermometry at 505 K and 693 K using quantized voltage noise ratio spectra,” in: *Proceedings of TEMPMEKO & ISHM 2010*, 31 May- 4 June 2010, Portorož, Slovenia, Joint International Symposium on Temperature, Humidity, Moisture and Thermal Measurements in Industry and Science, International Journal of Thermophysics, vol. 31, no. 8, pp. 1719-1738, Sept. 2010. DOI: 10.1007/s10765-010-0830-9.

[27] Benz S P, Dresselhaus P D, and Burroughs C J, “Multitone waveform synthesis with a quantum voltage noise source,” IEEE Trans. Appl. Supercond., vol. 21, no. 3, pp. 681 - 686 Jun. 2011.

[28] Urano C et al., “Johnson noise thermometry based on integrated quantum voltage noise source," *IEEE Trans. Appl. Supercond.*, vol. 26, no. 3, pp. 1800305-5, Apr. 2016.

[29] Benz S P, Pollarolo A, Qu J, Rogalla H, Urano C, Tew W L, Dresselhaus P D, and White D R, “An electronic measurement of the Boltzmann constant,” Metrologia, vol. 48, pp. 142-153, March 2011.

[30] Benz S P, “Quantum-based Voltage Waveform Synthesis,” in “Metrology” chapter in *100 Years of Superconductivity*, H. Rogalla and P. Kes, eds., Brussels: Chapman & Hall // CRC Press of the Taylor & Francis Group, 2011, pp. 546-552.

[31] Benz S P, Hamilton C A, A pulse-driven programmable Josephson voltage standard, Appl. Phys. Lett. 68 (1996) 3171-3173.

[32] Benz S P and Waltman S B, “Pulse-bias electronics and techniques for a Josephson arbitrary waveform synthesizer,” *IEEE Trans. Appl. Supercond.*, vol. 24, no. 6, pp. 1400107-6, July 2014. DOI: 10.1109/TASC.2014.2338326.

[33] Zhou K, Qu J, and Benz S P, “Zero-compensation method and reduced inductive voltage error for the ac Josephson voltage standard,” *IEEE Trans. Appl. Supercond.*, vol. 25, no. 5, pp. 1400806-6, Aug. 2015 DOI: 10.1109/TASC.2015.2470684

[34] White D R and Mason R S, An EMI test for Johnson noise thermometry, Proc. TEMPMEKO 2004 (Faculty of Mechanical and Naval Architecture, Zagreb, Croatia) ed D Zvizdic et al pp 485–90

[35] White D R and Zimmermann E, Preamplifier limitations on the accuracy of Johnson noise thermometers, *Metrologia*, 2000, **37**, 11-23

[36] White D R, Non-linearity in Johnson noise thermometry, *Metrologia* 49 (2012) 651–665